

Optical control of the moiré twist angle

Zhiren He,¹ Prathap Kumar Jharapla,² Nicolas Leconte,² Jeil Jung,² and Guru Khalsa¹

¹Department of Physics, University of North Texas, Denton, TX 76203, USA

²Department of Physics, University of Seoul, Seoul 02504, Korea

(Dated: March 2025)

Moiré multilayers offer a promising platform for engineering diverse functionalities in a single material via twist angle control. However, achieving reliable, high-precision control of the twist angle remains challenging. In this theoretical work, we propose an all-optical method for fast, precise manipulation of two-dimensional multilayers by transferring orbital angular momentum from phase-structured light (e.g. vortex beams) to a 2D material flake. We model the light-matter interaction, analyze the twist dynamics, and develop a phase diagram for optical twist angle switching – transition to a neighboring metastable twist angle – by mapping the system onto an impulsively forced nonlinear pendulum. Aided by pairwise classical potential estimates for the interlayer energy and numerical simulation, we demonstrate the feasibility of our approach with hexagonal boron nitride bilayers and extend the results to dichalcogenides with first-principles calculations. Our findings reveal a rich dynamical response – from single-pulse twist angle control to high-order quasistable orbits pointing toward periodically driven chaotic dynamics – and suggest a pathway for all-optical measurement of the twist potential energy. These results can be generalized to other 2D multilayers, paving the way for scalable and customizable moiré electronics and photonics.

Introduction—The sensitivity of the band structure and associated correlation effects to twist angle in two-dimensional materials offers a powerful handle for engineering novel quantum phases and functionalities [1–4]. However, this sensitivity also presents a significant challenge, as the exploration of electronic and optical properties relies heavily on the fabrication of high-quality moiré multilayers with precise control over twist angle. The earliest method of tear and stack [5] resulted in random twist angles that were not tunable. Various advanced assembly and twisting techniques have followed, including the manipulation of twist angle by scanning microscopes [6–8], the cutting-rotation-stacking method [9], mechanical bending [10], and a recent approach based on an electrostatic micro-electromechanical system (MEMS) [11]. Despite these advancements, these techniques still require sophisticated nano-fabrication/transfer processes, limiting scalability, reproducibility, and *in-situ* tunability.

Spatially phase-structured light, such as a vortex beam, carries orbital angular momentum (OAM), providing an optical handle on the twist angle. Vortex beams have been used to rotate macroscopic objects like μm -sized beads or even three-dimensional optically trapped structures [12–15]. Vortex beams are traditionally generated using light in the near-infrared (IR) to visible range, where they primarily couple to electronic degrees of freedom. However, recent advances have extended their reach into the mid- and far-IR regimes [16–18]. In parallel, powerful laser sources in these frequency ranges have demonstrated significant potential for lattice and structural control [19–24], yet vortex beams have not been explored for this purpose. Recent theoretical studies have proposed using terahertz vortex beams to manipulate topological spin and polar textures [25, 26], suggesting that mid- and far-IR vortex beams could soon play a role

in structural control and the manipulation of correlated phenomena.

In this Letter, we conceptualize an optical strategy for tuning the twist angle with OAM-carrying vortex beams in the mid- and far-IR, as shown in Fig. 1. The OAM of light is efficiently converted to mechanical rotation of two-dimensional (2D) flakes through resonant excitation of an IR-active phonon. We propose a strategy with the following key-features: (1) pristine moiré multilayers can be directly manipulated without additional fabrication steps or direct contact, whether *in situ* or *in vacuo* and (2) a wide range of twist angles are accessible and tunable on a fast timescale.

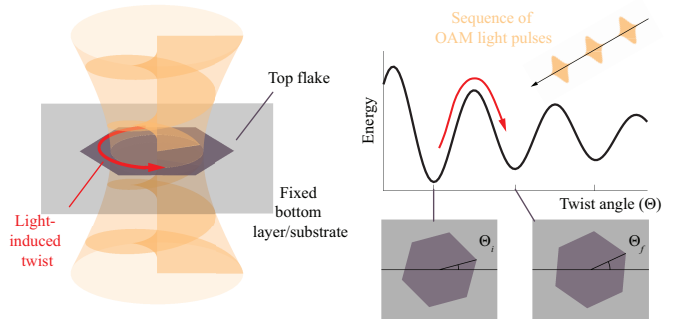


FIG. 1. **Schematic of the optical twisted process.** Left: A flake of 2D material situated on a surface/substrate gains angular momentum from a spatially phase-structured optical pulse (e.g. vortex beam; orange). Right: The optically applied torque from a single, or a series of, optical pulses overcome a barrier in the twist potential energy landscape, rotating the flake to a new twist angle.

In what follows, we first illustrate the light-matter interaction in a general sense, showing that our strategy is applicable to many moiré homo/heterostructures. We

then explore the twist dynamics of a 2D flake where we find rich dynamical response regimes and derive analytic results to guide experimental test of this proposal. Then using hexagonal boron nitride (hBN) as a case study, we combine pairwise classical potential results with numerical simulations to quantitatively validate the feasibility of our approach. Finally, the analysis is extended to moiré transition metal dichalcogenides (TMDs).

Torque Generation with Phase-Structured Light — Circularly polarized light is the most common source of light’s angular momentum used in measurement and technology. This *spin angular momentum* (SAM) arises from the rotation of the uniform polarization plane. By spatially structuring the phase of the wavefront, *orbital angular momentum* (OAM) can be imparted to light. Here we briefly describe OAM in Laguerre-Gaussian (LG) beams of light and their transfer of angular momentum to the lattice of a stack of 2D materials, noting that other phase-structured OAM light will follow the same principles *mutatis mutandis*.

Suppose that a moiré multilayer is placed near the beam’s focal point ($z = 0$). The LG beam’s spatial profile in cylindrical coordinate (r, ϕ, z) is

$$u(r, \phi, z = 0) = \frac{C_{\ell p}^{LG}}{w_0} \left(\frac{r\sqrt{2}}{w_0} \right)^{|\ell|} L_p^{|\ell|} \left(\frac{2r^2}{w_0^2} \right) e^{-r^2/w_0^2} e^{-i\ell\phi} \quad (1)$$

where

$$C_{\ell p}^{LG} = \sqrt{\frac{2p!}{\pi(p + |\ell|)!}}$$

is a normalization factor, w_0 is the beam waist radius and $L_p^{|\ell|}(x)$ is the associated Laguerre polynomial in x of order $|\ell|$ and degree p . Here, OAM is indexed by ℓ , derived from the phase structure $e^{-i\ell\phi}$, with negative/positive ℓ labeling angular momentum vectors parallel/antiparallel with the light’s propagation vector. The index $p \geq 0$ labels the number of radial nodes in the beam’s spatial profile. (We take $p = 0$ in what follows.) In addition to the OAM, SAM can be added by constructing a circularly polarized beam, i.e. $\vec{E} = E_0 u(r, \phi, z)(\hat{x} \pm i\hat{y})$. OAM and SAM are additive and LG beam with frequency ω has a well-defined time-averaged total angular momentum density per unit power of [27]

$$J = \frac{\ell + s}{\omega} |u|^2. \quad (2)$$

where $s = 0, \pm 1$ for linear and circular polarization, respectively.

A vortex beam passes its angular momentum to matter via absorption processes. Although large optical absorption can be achieved by exciting transitions between electronic bands, we expect it to be an inefficient route for angular momentum transfer in typical materials as this

mechanism relies on, the often small, electron-phonon coupling channels. Therefore, transferring the angular momentum to the lattice *directly* by exciting the IR-active phonon may prove to be a better strategy, especially near the IR resonance, where absorption of mechanical energy is maximized.

A microscopic view of the angular momentum transfer process at resonance is shown in Fig. 2 for a 2D hexagonal flake. The time evolution of the spatial profile for $\ell = 1, p = 0$ LG beam is illustrated in the first row. The nonuniform electric field of the LG beam induces a 2D polarization texture $\mathbf{P}(x, y) = \tilde{Z}^* \mathbf{Q}_{\text{IR}}(x, y)/A_0$ through the displacement of in-plane polarized IR-active phonons. Here, \mathbf{Q}_{IR} is the induced amplitude of the IR-active phonon and \tilde{Z}^* is the mode-effective charge dictating the coupling strength per unit cell area A_0 . When driven on resonance, the phase of the IR-active phonon and induced electric polarization \mathbf{P} will lag behind the electric field by a quarter period, as is seen in the resonant drive of a damped-driven harmonic oscillator. \mathbf{P} creates bound charges on both the bulk ($\rho_b = \nabla \cdot \mathbf{P}$) and the boundary ($\sigma_b = \hat{n} \cdot \mathbf{P}$, \hat{n} being the edge normal) of the flake which varies in time with the period of the electric field. The field-induced charges generate torque that acts directly on the lattice

$$\boldsymbol{\tau} = \int dA \mathbf{r} \times (\rho_b + \sigma_b a_0/A_0) \mathbf{E}(x, y) e^{-i\phi}, \quad (3)$$

where a_0 is the lattice constant, $\phi = \pi/2$ describes the phase lag, and the integral is over some areal region of the flake. In Fig. 2, the total torque is positive throughout the electric field period, though a small weak negative component can be seen near the boundary, a consequence of the linear polarization. A more uniform torque can be generated by circularly polarized LG pulses [28]. The time-averaged torque profile, proportional to the intensity profile, has only radial dependence, which can be adjusted by beam characteristics through ℓ and p , and w_0 .

Using this angular momentum transfer mechanism, we demonstrate that a sequence of ultra-short pulses of vortex beams in the mid-/far-IR can overcome the twist energy needed to change the relative interlayer twist angle.

Modeling the Twist Dynamics—A single layer has access to a broad range of stable angles which depend on the relative alignment with the underlying multilayer or substrate, suggesting a corrugated potential energy landscape parameterized by twist angle Θ . Near any metastable reference twist angle, the potential energy landscape can be reasonably approximated as a sinusoidal function,

$$U(\Theta) = \frac{1}{2} U_0 [1 - \cos(k\Theta)]. \quad (4)$$

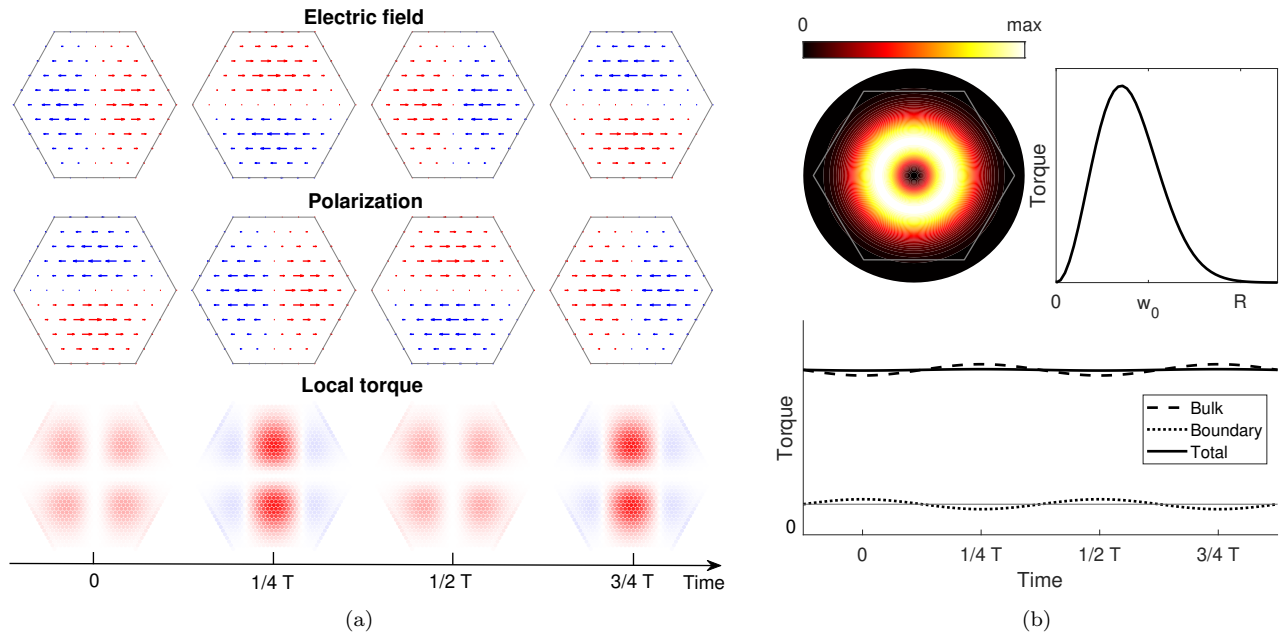


FIG. 2. **Torque generation via vortex beam-matter interaction.** (a) Quarter-period snapshots of the distribution of electric field, electric polarization, and torque when a linearly polarized Laguerre-Gaussian vortex beam ($\ell = -1$, $p = 0$, $w_0 = 0.5R$) resonantly excites an IR-active phonon in a hexagonal flake. Left and right electric field/polarization directions are represented by blue and red arrows, respectively, with lengths proportional to the magnitude. For local torque, positive/negative torque is shown in red/blue with torque magnitude proportional to the color saturation. (b) Radial dependence of the time-averaged torque distribution from (a) (Top). Time variation of the integrated total torque, compared with the flake bulk and boundary (Bottom).

To access a neighboring twist angle minima from any reference metastable point, a barrier of height U_0 must be overcome. Here, k parameterizes the local potential energy so that neighboring energy minima are separated by $\pm 2\pi/k$. Displacing the angle Θ from equilibrium gives a restoring torque $\tau(\Theta) = -\partial_{\Theta}U(\Theta) = -\tau_0 \sin(\Theta)$, where $\tau_0 = kU_0/2$. The dynamics can thus be modeled in analogy to a rigid pendulum, with a moment of inertia I describing the distribution of mass about the rigid flake's rotation center, and resonant frequency $\Omega_0 = \sqrt{k^2 U_0 / 2I}$ when Θ is small. Defining a rescaled coordinate $\Theta' = k\Theta$, we see that within this picture, access to a new twist angle is analogous to a rigid pendulum traversing its highest point, i.e. when Θ' crosses $\pm\pi$.

We thus model the twist dynamics by a damped-driven nonlinear pendulum equation,

$$\frac{d^2\Theta'}{dt^2} + \gamma \frac{d\Theta'}{dt} + \Omega_0^2 \sin \Theta' = \tau(t)/I \quad (5)$$

where γ is the effective damping parameter and $\tau(t)$ is a driving torque which can be derived[28] from Eqn. 3 or energy considerations with Eqn. 2.

As the flake rotates about the center, its motion at the edge is limited by the speed of sound v_s . This suggests a lower bound for the twist angle period given by $T_0 =$

$2\pi/\Omega_0 \sim v_s/R \approx 10$ ns, for a flake of radius $R \sim 100$ μm and $v_s \sim 10^4$ m/s. Conversely, mid- and far-infrared laser pulses are typically prepared with fs or ps duration. This suggests that the torque induced by the OAM light pulse on a flake of 2D material is *impulsive* and given by

$$\tau(t) = 2I\Omega_0 J' \sum_n \delta(t - t_n) \quad (6)$$

where t_n is the arrival time of each LG pulse and J' is the ratio of the angular momentum transferred from the optical pulse to the flake to the angular momentum required to reach the potential energy maximum, $J_0 = 2I\Omega_0/k$. We find,

$$J' = \left[\frac{\ell + s}{\omega} (\Gamma_{abs} F A_{flake}) \right] / \left(\frac{2I\Omega_0}{k} \right) \equiv \frac{J_{optic}}{J_0} \quad (7)$$

In this expression, J_{optic} is the total angular momentum gained by a flake with size A_{flake} from light, with fluence F and absorption ratio Γ_{abs} . With switching in mind, this is naturally compared to the angular momentum J_0 derived from the energy barrier U_0 .

The impulsively driven dynamics described by Eqn. 5 lead to rich dynamical behavior and the potential for chaos [29]. Here, we focus our exploration on the conditions required to overcome the local potential barrier.

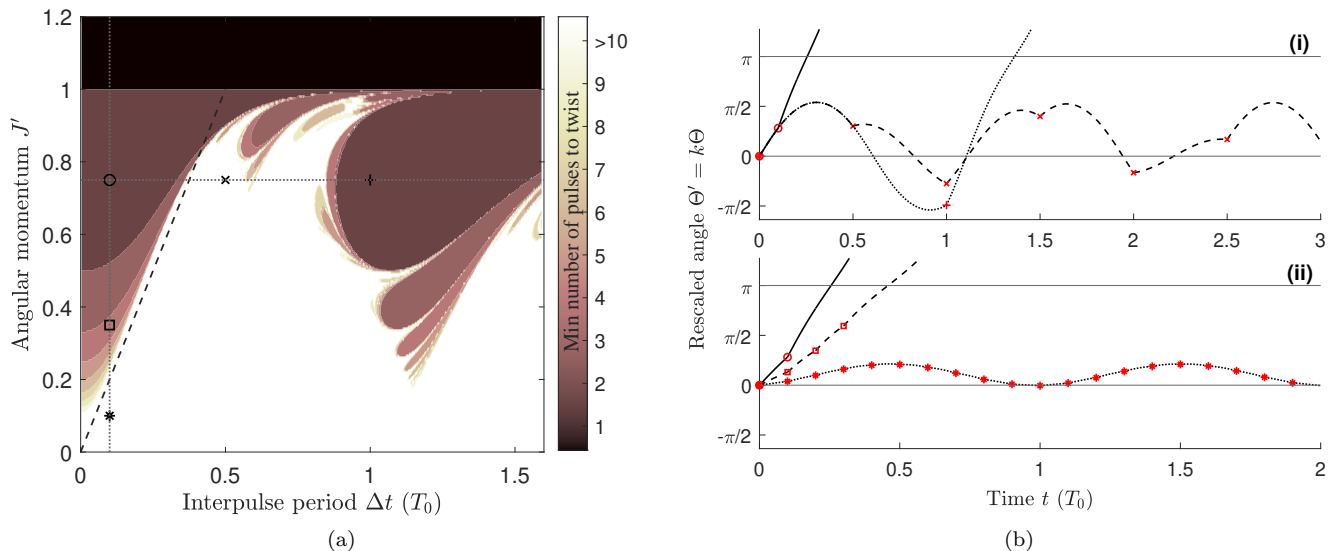


FIG. 3. (a) Contour plot of the minimum number of pulses required to overcome a local twist potential energy barrier versus J' – the ratio of the angular momentum transferred from the optical pulse to the flake to the angular momentum required to reach the potential energy maximum – and interpulse period Δt . When $J' > 1$, a single pulse is enough to twist the flake. For $J' < 1$, tongues emerge near integer multiples of the flake period T_0 . The intrinsic nonlinearity of the restoring torque leads to a redshift of the switching condition and the appearance of sub-tongues showing self-similarity, suggestive of the approach to chaos. (b) Selected dynamics in the low repetition rate (i) and high repetition rate (ii) regimes. In the low repetition rate regime, the optical torques must be timed to work in concert with the motion of the flake. In the high repetition rate regime, the time-averaged optical torque pushes the twist angle toward the barrier, overcoming it when $J' \geq 2\Delta t/T_0$.

We illustrate the twist dynamics for a sequence of evenly spaced LG pulses. By numerically integrating Eqn. 5 the minimum number of pulses required for the flake to overcome the twist energy barrier (i.e. when $|\Theta'| > \pi$) can be tracked. Fig. 3(a) shows this result with respect to J' and the interpulse period $\Delta t/T_0 = (t_{n+1} - t_n)/T_0$ scaled by the intrinsic period of the referenced metastable energy well, in the limit of no damping. Including damping shifts the contour lines up in Fig. 3a because more energy will be dissipated from the system. This effect becomes more dramatic at larger $\Delta t/T_0$ due to the increased travel time between optical torques, though the qualitative features remain unchanged[28].

We select several representative points in the phase diagram to illustrate the rich twist dynamics (Fig. 3(b)). For high repetition rate, many impulsive torques are applied to the flake within a single period of motion. This suggests that the flake experiences a time-averaged torque of $2I\Omega_0 J'/\Delta t$, where $1/\Delta t$ is the repetition rate of the laser. The need for this time-averaged drive to overcome the barrier energy defines a condition $J' \geq 2\Delta t/T_0$, which sets a bound on the laser characteristics required for switching in the high repetition rate regime[28]. Below this threshold, oscillatory motion is expected about a shifted minimum; above this threshold, switching occurs.

As the interpulse period Δt increases, we move through an out-of-phase drive region where switching requires fluence comparable to the single pulse threshold value.

When the interpulse period is comparable to MT_0 , for some positive integer M , we expect that periodic drive should again cause large amplitude twists. But larger amplitudes experience a weaker restoring torque due to the sinusoidal variation of the twist potential energy. This leads to a red shift in the frequency to above Ω_0 . The tongue (shaded region) can be seen extending toward $\Delta t/T_0 \approx 1.2$ in Fig. 3. In this region, switching is still possible, but the periodic optical torque must work in concert with the angular velocity to overcome the restoring torque. Without carefully timing the optical pulses, the system can remain in driven oscillatory motion for very long times. The structured, self-similar sub-tongues are also prominent in Fig. 3a. These sub-tongues become increasingly narrow for longer pulse-sequences switching conditions, while interpenetrating white regions persist, supporting high-order (quasi) stable orbits within the potential energy well. This hierarchical pattern signals a gradual transition toward chaotic behavior whose detailed exposition is beyond the scope of this work.

With the general dynamics and the conditions for switching in hand, we now explore hBN as a representative candidate for optical control of moiré twist angle, illustrating the feasibility and limitations of this approach.

hBN case study—To assess the feasibility of our approach, we need to calculate or approximate J' . Because hBN shows moiré physics and has a doubly-degenerate in-plane polarized IR-active phonon, it should

be amenable to the optical twisting process. To estimate J' we need only the potential energy variation with Θ and the absorption at the pumped phonon resonance.

We calculate the potential energy as a function of twist angle for a rigid flake of radius R on an extended and pinned layer of hBN. This is done by summation of all of the pairwise interlayer interactions following

$$E_{\text{tot}} = \frac{1}{2} \sum_i \sum_{j \notin \text{layer } i} \phi_{ij} \quad (8)$$

where N corresponds to the number of atoms and where ϕ_{ij} is given by the DRIP potential functional [30] with reparameterization [31] using EXX-RPA data [32]. We define the orientation of the layers so that AA-stacking is $\Theta = 0$.

Figure 4 summarizes the results for a hexagonal flake with armchair edges. We find that the energy landscape is qualitatively similar to the physically motivated result of Eqn. 4 locally, except for a weakly varying background and a beating pattern. As expected, we find that the number of stable angles increases with radius. For small angles (near AA stacking), the energetic barrier between neighboring minima also increases. The falloff in barrier height with angle is dramatic, quickly transitioning to a regime where a beat pattern emerges beyond a critical angle $\Theta_c(R) \approx 74/\sqrt{a_0/R}$. This beating pattern is a consequence of the specific orientation of the moiré pattern with respect to the edges of the flake, signaling the importance of the relative distribution of stable and unstable local stacking configurations at the edges [33–36]. We note that when choosing AB-stacking as the rotation center, the energetics are equivalent except with a phase shift in the oscillation [28]. Interestingly, beyond $\Theta_c(R)$ in the *large angle* regime, the maximum barrier height within a beat becomes independent of radius, depending only on the angle. We find that the potential energy can be approximated locally with Eqn. 4, with an *upper bound* on the barrier height $U_0(\Theta) = 2A\Theta^{-3}$, where $A \approx 717.3$ eV. The angular scaling parameter is proportional to flake radius, but independent of the twist angle, i.e. $k = bR/a_0$, where $b \approx 0.1103$.

Using these results, we find that the resonant frequency and dimensionless torque can be approximated as

$$\Omega_0 = \sqrt{\frac{k^2 U_0}{2I}} = \sqrt{\frac{2Ab^2}{\pi \rho a_0^2}} \frac{\Theta^{-3/2}}{R} \quad (9)$$

and

$$J' = \frac{\ell + s}{\omega} \sqrt{\frac{\pi}{2\rho A}} \Gamma_{\text{abs}} F \Theta^{3/2}, \quad (10)$$

respectively, using a circular flake ($I = 1/2\pi\rho R^4$) for simplicity.

Whereas directly simulating a flake size comparable with electronic and optical device fabrication needs (i.e.

$\sim 100 \mu\text{m}$) is too cumbersome, our findings can be extrapolated from the simulation geometries to any desired scale. For a circular hBN flake of radius = 100 μm , absorption $\Gamma_{\text{abs}} = 0.1$, vortex beam carrier frequency $\omega = 2\pi \times 40.3$ THz, $\ell = 1$, $s = 0$, and fluence $F = 50$ mJ/cm², we find $J' = 0.022 \Theta^{3/2}$. This gives the single-pulse switching boundary in Fig. 3 (i.e. $J' = 1$) at $\Theta \approx 12.7^\circ$. The flake's natural frequency is then $\Omega_0 \approx 76.8 \Theta^{-3/2}$ MHz, corresponding to an oscillation period of $T_0 \approx 81.8 \Theta^{3/2}$ ns, comparable to our initial estimates. Above this angle, we anticipate single-pulse switching. Below this angle, we anticipate that a sequence of pulses will be necessary for moiré twist angle switching. Additionally, the dynamics portrayed in Fig. 3 can be explored below this angle.

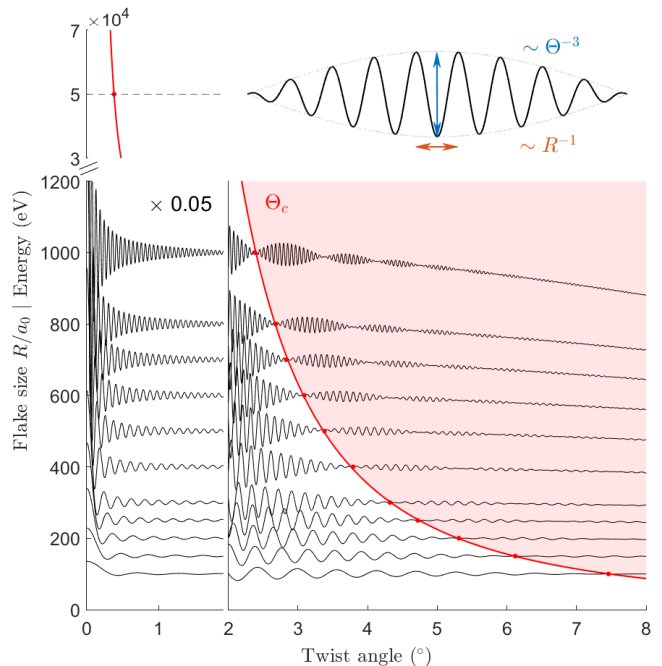


FIG. 4. **Total energy versus twist angle and flake radius for hBN on hBN.** Each line is shifted so that its origin is the flake radius and the variation from the origin is the total energy versus angle. For angles below 2° the energy is rescaled by a factor of 20. The red line shows the critical angle Θ_c – the transition from the *low-angle* to *high-angle* regimes. In the high-angle regime (shaded region), the barrier height becomes independent of the flake radius, depending only on angle as Θ^{-3} . Extrapolating to large flake radii shows that the high-angle regime will dictate the twist barrier for macroscopic flakes (i.e. $R \sim 100 \mu\text{m}$) for most starting angles.

Discussion and Generalization — The utility of the theoretical exposition in this work relies on the calculation of the twist potential energy for a flake of 2D material. The twist potential energy can alternatively be constructed from geometrical insights. The realization is that it should depend on the relative areas of AA- and AB-stacked regions. This enables a theoretical estimate

	hBN	MoS ₂	MoSe ₂	MoTe ₂
a (Å)	2.505	3.161 [37]	3.288 [38]	3.519 [39]
ρ (AMU/Å ²)	4.57	18.50	27.12	32.74
$\omega/(2\pi)$ (THz)	40.3	8.55, 11.53	5.04, 8.60	3.56, 7.13
E(AA)-E(AB) (meV)	27.2	72.5	82.6	113.0
J' (MoX ₂)/ J' (hBN)	–	1.43, 1.06	1.88, 1.10	2.08, 1.04
Ω_0 (MoX ₂)/ Ω_0 (hBN)	–	0.51	0.42	0.39

TABLE I. Estimation of J' – the ratio of the angular momentum transferred from the optical pulse to the flake to the angular momentum required to reach the potential energy maximum – and resonance frequency Ω_0 for TMDs, compared with hBN. a is the lattice constant, ρ is the mass density, ω is the frequency of IR-active phonon in the plane. For MoX₂, there are 2 IR-active phonons. E(AA)-E(AB) is the energy difference between the AA and AB stacking order.

for the possibility of optical control of twist angles in other 2D materials without cumbersome computations. We take the scaling relation $U_0(\Theta) = 2A\Theta^{-3}$ to be general, since it stems from the weak interlayer interaction, a general feature/necessary ingredient for 2D materials amenable to twisted moiré patterning. We can then estimate the coefficient A as the energy difference between the stacking configurations, i.e. $A \propto E(AA) - E(AB)$, a quantity readily found by conventional techniques.

Under the same total angular momentum $\ell + s$, absorption coefficient Γ_{abs} , and twist angle Θ , a comparison of J' and Ω_0 between hBN and MoX₂ becomes possible (TABLE I). Although MoX₂ flakes are heavier and exhibit larger twist barriers than hBN, these estimates suggest that they may be easier to twist than hBN. This is a consequence of the OAM density's inverse proportionality in frequency ω (Eq. 2). For the same flake radius R , MoX₂ flakes also have lower natural frequencies Ω_0 . The combination of higher J' and lower Ω_0 suggests that the single-pulse switching boundary and tongue regions in Fig. 3 are more accessible for MoX₂ flakes, provided similar pulse characteristics can be achieved at these pump frequencies.

A successful optical twist may require much less power than estimated in this work. This follows from thermal expansion and fluctuations weakening the interlayer coupling, possible adsorbates in fabricated samples, and the rigid flake approximation. We anticipate that as the temperature is increased from the zero temperature simulation value to room temperature or higher through substrate heating in experimental conditions, the interlayer distance will increase, lowering the effective interlayer coupling and moving the single-pulse switching boundary ($J' = 1$) to smaller angles.

Concurrently, real samples are not pristine; they may have adsorbates or leftover polymers from the transfer process, defects, twist-disorder, and wrinkles which may alter the interlayer coupling. Finally, OAM light converted to the infrared are already used to ablate and laser-etch covalent materials in fabrication processes. Therefore, although our estimates for hBN suggests single-pulse control achievable only at large angles, exist-

ing laser source may be readily deployable with modest effort for OAM light construction in the mid- and far-IR.

Additionally, the rigid flake approximation assumes that the whole sample moves together. But, following the reasoning for our estimates of Ω_0 above through acoustic velocity, we anticipate that the rotation will be carried by propagating domain walls between twisted stacking faults of neighboring angular regions. It follows that spatially phase-structured light may be used to manipulate these domains and remove twist disorder or other defects, pushing samples toward the pristine single-angle limit. This precise control and homogeneity of the twist angle may be especially important for homo-multilayers where correlated physics only appears in a narrow angular range.

Relaxation may also affect the barrier to switching and light-induced dynamics. Often, the barrier between two nearby nuclear configurations are *overestimated* by rigid dynamics. Because the twist dynamics are likely carried by the motion of stacking fault domain walls expected to travel at the speed of sound, and the optical torque is impulsive, the induced dynamics may also depend on relaxation effects. Notably, complex relaxation effects including angular and strain disorder, atomic reconstruction, twin-domains in 2D multilayers have been reported [40–46]. This suggests that resolving the micro-/mesoscopic structural changes in this broad temporal range may require technique and tool development on both theoretical and experimental fronts.

With these considerations, since OAM light can excite the rotational degrees of freedom, direct optical study and measurement of the twist potential and fast (sub-nanosecond) twist dynamics become possible. This opens up new avenues for exploration of the fundamental physics of angular momentum transfer and relaxation dynamics in 2D materials.

In addition to the implications for moiré materials, generally, there are several implications directly applicable to hBN efforts. Twisted hBN gives rise to narrow low-energy bands [47] and has attracted significant interest due to its interfacial local layer ferroelectricity, which can be switched by a perpendicular electric field [48–54]. This tunability provides a mechanism to modify the elec-

tronic properties of adjacent 2D material layers through a proximity effect [55, 56].

The armchair edge configurations studied in this work shows higher energy barriers than zigzag edge termination[33]. A similar study on graphene shows that edge configuration affects the equilibrium energy of small round and hexagonal flakes [57]. This suggests the possibility of edge-engineering as a strategy for enabling twist reconfiguration of hBN flakes, particularly in the high-angle regime. This has implications for optically controlled twist angle, but, if controlled, may also influence rotational friction in nanodispersed hBN.

Conclusion—Our study presents an optical strategy

for fast, precise, and potentially scalable control of the moiré twist angle in 2D multilayers through the use of OAM-carrying vortex beams in the mid- and far-IR. The key physical realization is that OAM pulses can impart substantial angular momentum on large-scale 2D materials flakes through the excitation of IR-active phonons. This induces complex dynamics and switching, provided the interlayer potential energy/torque can be overcome. Using the example of hBN, we find that current laser sources are deployable to initiate the study of this strategy for moiré twist-angle control. Finally, this approach is readily generalized to a broad class of 2D materials.

Scaling the equation of motion

The complete equation of motion is

$$I \frac{d^2 \Theta}{dt^2} + I \gamma \frac{d\Theta}{dt} + \frac{1}{2} k U_0 \sin(k\Theta) = \frac{\ell}{\omega} (\Gamma_{abs} F A_{flake}) \sum_n \delta(t - t_n)$$

where

$$U_0 = \frac{2I\Omega_0^2}{k^2} = \frac{1}{2} I \left(\frac{2\Omega_0}{k} \right)^2.$$

From Eqn. 4, notice that if U_0 – the maximum potential energy difference – is converted to rotational kinetic energy, the angular momentum of the flake is

$$J_0 = I \left(\frac{2\Omega_0}{k} \right) = \frac{2I\Omega_0}{k}.$$

We first scale the twist angle $k\Theta \rightarrow \Theta'$,

$$\frac{I}{k} \frac{d^2 \Theta'}{dt^2} + \frac{I}{k} \gamma \frac{d\Theta'}{dt} + \frac{I\Omega_0^2}{k} \sin(\Theta') = \frac{\ell}{\omega} (\Gamma_{abs} F A_{flake}) \sum_n \delta(t - t_n)$$

then multiply both sides by k/I ,

$$\frac{d^2 \Theta'}{dt^2} + \gamma \frac{d\Theta'}{dt} + \Omega_0^2 \sin(\Theta') = \frac{k \ell}{I \omega} (\Gamma_{abs} F A_{flake}) \sum_n \delta(t - t_n). \quad (11)$$

We can scale it further by applying the transformation $\Omega_0 t \rightarrow t'$ and $\gamma/\Omega_0 \rightarrow \gamma'$:

$$\Omega_0^2 \frac{d^2 \Theta'}{dt'^2} + \Omega_0^2 \gamma' \frac{d\Theta'}{dt'} + \Omega_0^2 \sin(\Theta') = \frac{k \ell}{I \omega} (\Gamma_{abs} F A_{flake}) \sum_n \Omega_0 \delta(t' - t'_n)$$

Divide both sides by Ω_0^2 :

$$\frac{d^2 \Theta'}{dt'^2} + \gamma' \frac{d\Theta'}{dt'} + \sin(\Theta') = \frac{k \ell}{I \Omega_0 \omega} (\Gamma_{abs} F A_{flake}) \sum_n \delta(t' - t'_n) = 2J' \sum_n \delta(t' - t'_n)$$

where

$$J' = \frac{\ell/\omega (\Gamma_{abs} F A_{flake})}{2I\Omega_0/k} = \frac{J_{optic}}{J_0}$$

compares the flakes angular momentum gained from light with that derived from the energy barrier. This suggests a rewriting of Eqn. 11 as

$$\frac{d^2 \Theta'}{dt'^2} + \gamma' \frac{d\Theta'}{dt'} + \sin(\Theta') = 2\Omega_0 J' \sum_n \delta(t - t_n).$$

deriving the form of Eqn. 5 and Eqn. 6.

-
- [1] R. Bistritzer and A. H. MacDonald, Moiré bands in twisted double-layer graphene, *Proceedings of the National Academy of Sciences* **108**, 12233 (2011).
 [2] E. Y. Andrei, D. K. Efetov, P. Jarillo-Herrero, A. H. MacDonald, K. F. Mak, T. Senthil, E. Tutuc, A. Yazdani, and A. F. Young, The marvels of moiré materials, *Nature Reviews Materials* **6**, 201 (2021).
 [3] K. F. Mak and J. Shan, Semiconductor moiré materials, *Nature Nanotechnology* **17**, 686 (2022).

- [4] L. Du, M. R. Molas, Z. Huang, G. Zhang, F. Wang, and Z. Sun, Moiré photonics and optoelectronics, *Science* **379**, 10.1126/science.adg0014 (2023).
- [5] K. Kim, M. Yankowitz, B. Fallahazad, S. Kang, H. C. P. Movva, S. Huang, S. Larentis, C. M. Corbet, T. Taniguchi, K. Watanabe, S. K. Banerjee, B. J. LeRoy, and E. Tutuc, van der waals heterostructures with high accuracy rotational alignment, *Nano Letters* **16**, 1989–1995 (2016).
- [6] R. Ribeiro-Palau, C. Zhang, K. Watanabe, T. Taniguchi, J. Hone, and C. R. Dean, Twistable electronics with dynamically rotatable heterostructures, *Science* **361**, 690 (2018).
- [7] C. Hu, T. Wu, X. Huang, Y. Dong, J. Chen, Z. Zhang, B. Lyu, S. Ma, K. Watanabe, T. Taniguchi, G. Xie, X. Li, Q. Liang, and Z. Shi, In-situ twistable bilayer graphene, *Scientific Reports* **12**, 10.1038/s41598-021-04030-z (2022).
- [8] Y. Yang, J. Li, J. Yin, S. Xu, C. Mullan, T. Taniguchi, K. Watanabe, A. K. Geim, K. S. Novoselov, and A. Mishchenko, In situ manipulation of van der waals heterostructures for twistrionics, *Science Advances* **6**, 10.1126/sciadv.abd3655 (2020).
- [9] X. Chen, W. Xin, W. Jiang, Z. Liu, Y. Chen, and J. Tian, High-precision twist-controlled bilayer and trilayer graphene, *Advanced Materials* **28**, 2563 (2016).
- [10] M. Kapfer, B. S. Jessen, M. E. Eisele, M. Fu, D. R. Danielsen, T. P. Darlington, S. L. Moore, N. R. Finney, A. Marchese, V. Hsieh, P. Majchrzak, Z. Jiang, D. Biswas, P. Dudin, J. Avila, K. Watanabe, T. Taniguchi, S. Ulstrup, P. Bøggild, P. J. Schuck, D. N. Basov, J. Hone, and C. R. Dean, Programming twist angle and strain profiles in 2d materials, *Science* **381**, 677 (2023).
- [11] H. Tang, Y. Wang, X. Ni, K. Watanabe, T. Taniguchi, P. Jarillo-Herrero, S. Fan, E. Mazur, A. Yacoby, and Y. Cao, On-chip multi-degree-of-freedom control of two-dimensional materials, *Nature* **632**, 1038 (2024).
- [12] L. Paterson, M. P. MacDonald, J. Arlt, W. Sibbett, P. E. Bryant, and K. Dholakia, Controlled rotation of optically trapped microscopic particles, *Science* **292**, 912 (2001).
- [13] M. P. MacDonald, L. Paterson, K. Volke-Sepulveda, J. Arlt, W. Sibbett, and K. Dholakia, Creation and manipulation of three-dimensional optically trapped structures, *Science* **296**, 1101 (2002).
- [14] D. G. Grier, A revolution in optical manipulation, *Nature* **424**, 810 (2003).
- [15] Y. Shen, X. Wang, Z. Xie, C. Min, X. Fu, Q. Liu, M. Gong, and X. Yuan, Optical vortices 30 years on: OAM manipulation from topological charge to multiple singularities, *Light: Science & Applications* **8**, <https://doi.org/10.1038/s41377-019-0194-2> (2019).
- [16] S. Araki, K. Ando, K. Miyamoto, and T. Omatu, Ultra-widely tunable mid-infrared (6-18 μm) optical vortex source, *Appl. Opt.* **57**, 620 (2018).
- [17] H. Tong, G. Xie, Z. Qiao, Z. Qin, P. Yuan, J. Ma, and L. Qian, Generation of a mid-infrared femtosecond vortex beam from an optical parametric oscillator, *Opt. Lett.* **45**, 989 (2020).
- [18] V. Sharma, S. C. Kumar, G. K. Samanta, and M. Ebrahim-Zadeh, Tunable, high-power, high-order optical vortex beam generation in the mid-infrared, *Opt. Express* **30**, 1195 (2022).
- [19] M. Först, C. Manzoni, S. Kaiser, Y. Tomioka, Y. Tokura, R. Merlin, and A. Cavalleri, Nonlinear phononics as an ultrafast route to lattice control, *Nature Physics* **7**, 854 (2011).
- [20] R. Mankowsky, A. von Hoegen, M. Först, and A. Cavalleri, Ultrafast reversal of the ferroelectric polarization, *Phys. Rev. Lett.* **118**, 197601 (2017).
- [21] D. M. Juraschek, M. Fechner, and N. A. Spaldin, Ultrafast structure switching through nonlinear phononics, *Phys. Rev. Lett.* **118**, 054101 (2017).
- [22] J. R. Hortensius, D. Afanasiev, A. Sasani, E. Bousquet, and A. D. Caviglia, Ultrafast strain engineering and coherent structural dynamics from resonantly driven optical phonons in LaAlO_3 , *npj Quantum Materials* **5**, <https://doi.org/10.1038/s41535-020-00297-z> (2020).
- [23] A. S. Disa, T. F. Nova, and A. Cavalleri, Engineering crystal structures with light, *Nature Physics* **17**, 1087 (2021).
- [24] G. Khalsa, J. Z. Kaaret, and N. A. Benedek, Coherent control of the translational and point group symmetries of crystals with light, *Phys. Rev. B* **109**, 024110 (2024).
- [25] L. Gao, S. Prokhorenko, Y. Nahas, and L. Bellaïche, Dynamical multiferroicity and magnetic topological structures induced by the orbital angular momentum of light in a nonmagnetic material, *Physical Review Letters* **131**, 196801 (2023).
- [26] L. Gao, S. Prokhorenko, Y. Nahas, and L. Bellaïche, Dynamical control of topology in polar skyrmions via twisted light, *Physical Review Letters* **132**, 026902 (2024).
- [27] L. Allen, M. W. Beijersbergen, R. J. C. Spreeuw, and J. P. Woerdman, Orbital angular momentum of light and the transformation of laguerre-gaussian laser modes, *Phys. Rev. A* **45**, 8185 (1992).
- [28] The supplementary material includes a description of LG beams with spin and orbital angular momentum; a derivation of the optical driving torque; the effect of damping on the phase diagram; a derivation of the high-repetition rate regime; the twist potential for the AB-stacking reference; and details of the fitting procedure and its quality.
- [29] A. S. de Paula, M. A. Savi, and F. H. I. Pereira-Pinto, Chaos and transient chaos in an experimental nonlinear pendulum, *Journal of Sound and Vibration* **294**, 585 (2006).
- [30] M. Wen, S. Carr, S. Fang, E. Kaxiras, and E. B. Tadmor, Dihedral-angle-corrected registry-dependent interlayer potential for multilayer graphene structures, *Phys. Rev. B* **98**, 235404 (2018).
- [31] N. Leconte, S. Javvaji, J. An, A. Samudrala, and J. Jung, Relaxation effects in twisted bilayer graphene: A multiscale approach, *Physical Review B* **106**, 115410 (2022).
- [32] N. Leconte, J. Jung, S. Lebègue, and T. Gould, Moiré-pattern interlayer potentials in van der waals materials in the random-phase approximation, *Phys. Rev. B* **96**, 195431 (2017).
- [33] J. Prathap kumar, N. Leconte, Z. He, G. Khalsa, and J. Jung, Strain engineering of stable angles between graphene flakes on hexagonal boron nitride, *In Preparation* (2025).

- [34] S. Zhu, P. Pochet, and H. T. Johnson, Controlling rotation of two-dimensional material flakes, *ACS Nano* **13**, 6925 (2019).
- [35] S. Zhu, E. Annevelink, P. Pochet, and H. T. Johnson, Selection rules of twistrionic angles in two-dimensional material flakes via dislocation theory, *Physical Review B* **103**, 115427 (2021).
- [36] W. Yan, W. Ouyang, and Z. Liu, Origin of frictional scaling law in circular twist layered interfaces: Simulations and theory, *Journal of the Mechanics and Physics of Solids* **170**, 105114 (2023).
- [37] B. Schönfeld, J. J. Huang, and S. C. Moss, Anisotropic mean-square displacements (msd) in single-crystals of 2h- and 3r-mos₂, *Acta Crystallographica Section B Structural Science* **39**, 404 (1983).
- [38] P. B. James and M. T. Lavik, The crystal structure of mose₂, *Acta Crystallographica* **16**, 1183 (1963).
- [39] D. Puotinen and R. E. Newnham, The crystal structure of mote₂, *Acta Crystallographica* **14**, 691 (1961).
- [40] A. Weston, Y. Zou, V. Enaldiev, A. Summerfield, N. Clark, V. Zólyomi, A. Graham, C. Yelgel, S. Magorrian, M. Zhou, J. Zultak, D. Hopkinson, A. Barinov, T. H. Bointon, A. Kretinin, N. R. Wilson, P. H. Beton, V. I. Fal'ko, S. J. Haigh, and R. Gorbachev, Atomic reconstruction in twisted bilayers of transition metal dichalcogenides, *Nature Nanotechnology* **15**, 592 (2020).
- [41] M. R. Rosenberger, H.-J. Chuang, M. Phillips, V. P. Oleshko, K. M. McCreary, S. V. Sivaram, C. S. Hellberg, and B. T. Jonker, Twist angle-dependent atomic reconstruction and moiré patterns in transition metal dichalcogenide heterostructures, *ACS Nano* **14**, 4550 (2020).
- [42] L. Brown, R. Hovden, P. Huang, M. Wojcik, D. A. Muller, and J. Park, Twinning and twisting of tri- and bilayer graphene, *Nano Letters* **12**, 1609 (2012).
- [43] J. S. Alden, A. W. Tsen, P. Y. Huang, R. Hovden, L. Brown, J. Park, D. A. Muller, and P. L. McEuen, Strain solitons and topological defects in bilayer graphene, *Proceedings of the National Academy of Sciences* **110**, 11256 (2013).
- [44] S. G. Xu, A. I. Berdyugin, P. Kumaravadivel, F. Guinea, R. Krishna Kumar, D. A. Bandurin, S. V. Morozov, W. Kuang, B. Tsim, S. Liu, J. H. Edgar, I. V. Grigorieva, V. I. Fal'ko, M. Kim, and A. K. Geim, Giant oscillations in a triangular network of one-dimensional states in marginally twisted graphene, *Nature Communications* **10**, 10.1038/s41467-019-11971-7 (2019).
- [45] H. Yoo, R. Engelke, S. Carr, S. Fang, K. Zhang, P. Cazeaux, S. H. Sung, R. Hovden, A. W. Tsen, T. Taniguchi, K. Watanabe, G.-C. Yi, M. Kim, M. Lusk, E. B. Tadmor, E. Kaxiras, and P. Kim, Atomic and electronic reconstruction at the van der Waals interface in twisted bilayer graphene, *Nature Materials* **18**, 448 (2019).
- [46] C. N. Lau, M. W. Bockrath, K. F. Mak, and F. Zhang, Reproducibility in the fabrication and physics of moiré materials, *Nature* **602**, 41 (2022).
- [47] L. Xian, D. M. Kennes, N. Tancogne-Dejean, M. Altarelli, and A. Rubio, Multiflat bands and strong correlations in twisted bilayer boron nitride: Doping-induced correlated insulator and superconductor, *Nano letters* **19**, 4934 (2019).
- [48] K. Yao, N. R. Finney, J. Zhang, S. L. Moore, L. Xian, N. Tancogne-Dejean, F. Liu, J. Ardelean, X. Xu, D. Halbertal, *et al.*, Enhanced tunable second harmonic generation from twistable interfaces and vertical superlattices in boron nitride homostructures, *Science Advances* **7**, eabe8691 (2021).
- [49] M. Vizner Stern, Y. Waschitz, W. Cao, I. Nevo, K. Watanabe, T. Taniguchi, E. Sela, M. Urbakh, O. Hod, and M. Ben Shalom, Interfacial ferroelectricity by van der waals sliding, *Science* **372**, 1462 (2021).
- [50] K. Yasuda, X. Wang, K. Watanabe, T. Taniguchi, and P. Jarillo-Herrero, Stacking-engineered ferroelectricity in bilayer boron nitride, *Science* **372**, 1458 (2021).
- [51] C. Woods, P. Ares, H. Nevison-Andrews, M. Holwill, R. Fabregas, F. Guinea, A. Geim, K. Novoselov, N. Walet, and L. Fumagalli, Charge-polarized interfacial superlattices in marginally twisted hexagonal boron nitride, *Nature communications* **12**, 347 (2021).
- [52] J. C. Rode, D. Smirnov, C. Belke, H. Schmidt, and R. J. Haug, Twisted bilayer graphene: interlayer configuration and magnetotransport signatures, *Annalen der Physik* **529**, 1700025 (2017).
- [53] S. Moore, C. Ciccarino, D. Halbertal, L. McGilly, N. Finney, K. Yao, Y. Shao, G. Ni, A. Sternbach, E. Telford, *et al.*, Nanoscale lattice dynamics in hexagonal boron nitride moiré superlattices, *Nature Communications* **12**, 5741 (2021).
- [54] G. Ni, H. Wang, B.-Y. Jiang, L. Chen, Y. Du, Z. Sun, M. Goldflam, A. Frenzel, X. Xie, M. Fogler, *et al.*, Soliton superlattices in twisted hexagonal boron nitride, *Nature communications* **10**, 4360 (2019).
- [55] D. S. Kim, R. C. Dominguez, R. Mayorga-Luna, D. Ye, J. Embley, T. Tan, Y. Ni, Z. Liu, M. Ford, F. Y. Gao, *et al.*, Electrostatic moiré potential from twisted hexagonal boron nitride layers, *Nature materials* **23**, 65 (2024).
- [56] F. Li, D. Lee, N. Leconte, S. Javvaji, Y. D. Kim, and J. Jung, Moiré flat bands and antiferroelectric domains in lattice relaxed twisted bilayer hexagonal boron nitride under perpendicular electric fields, *Phys. Rev. B* **110**, 155419 (2024).
- [57] T. Nakajima and K. Shintani, Molecular dynamics study of energetics of graphene flakes, *Journal of Applied Physics* **106**, 114305 (2009).

